Journal of Asian Ceramic Societies 1 (2013) 163–169

Journal of Asian Ceramic Societies

Journal of Asian Ceramic Societies

journal homepage: www.elsevier.com/locate/jascer

# Reaction sintered Fe–Sialon ceramic composite: Processing, characterization and high temperature erosion wear behavior

Jing-Zhou Yang[a,b], Zhao-Hui Huang[a,*], Ming-Hao Fang[a], Xiao-Zhi Hu[b], Yan-Gai Liu[a], Hao-Ran Sun[a]

[a] School of Materials Science and Technology, China University of Geosciences (Beijing), Beijing 100083, PR China
[b] School of Mechanical and Chemical Engineering, The University of Western, Australia, Perth, WA 6009, Australia

ARTICLE INFO

*Article history:*
Received 4 March 2013
Received in revised form 3 May 2013
Accepted 6 May 2013
Available online 23 May 2013

*Keywords:*
Ceramic matrix composites
Sialon
Ferro-silicon alloy
Reaction sintering
Erosion wear

ABSTRACT

Fe–Sialon ceramic matrix composite has been newly developed from ferro-silicon alloy and commercial-grade industrial alumina powders by reaction sintering under a nitrogen atmosphere. The phase composition, mechanical properties and impact erosion wear behavior were investigated. The solid particle erosion tests have been conducted at elevated temperatures ranging from 25 °C to 1200 °C. Sharp SiC particles between 325 and 830 μm in diameter were employed as impact abrasives. The results showed that Fe–Sialon ceramic consisted of β-Sialon and $Fe_3Si$ phases. The *Z* value of the as-formed β-Sialon varied from 0 to 3.2 with increasing the alumina content in the starting powders. The bending strength and Rockwell hardness gradually increased with raising the alumina addition. The erosion rate of Fe–Sialon ceramic is highly dependent on the testing temperature. The minor erosion took place at room temperature or 1200 °C, while the major erosion occurred at 600–1000 °C. Fe–Sialon composites showed better erosion wear resistance than the control material of alumina ceramic at 1200 °C, although having much lower density and slightly lower bending strength.



## 1. Introduction

Excellent high-temperature erosion-wear resistance is required for Sialon based ceramics used as wear resistant linings in the fields of metallurgical industry, coal-fired power station, cement producing, mineral exploring, and so forth. A few publications are available on the sliding and grain abrasive wear behaviors of Sialon based ceramics [1–8], but little work has been done on high-temperature erosion resistance and associated material removal mechanisms. The room-temperature erosion behaviors of Sialon ceramics have been reported and it is demonstrated that the erosion resistance of Sialon ceramics highly depends on their microstructures and some key mechanical properties [9–11]. As expected, high hardness and toughness help to improve the erosion resistance and a proper amount of intergranular glass phase and interlocking elongated grains is also beneficial to the erosion resistance. However, the erosion-wear behavior of ceramics would change to some extent at high temperatures. This paper will focus on the high temperature erosion-wear behavior of a newly developed Sialon matrix ceramic.

In addition, Sialon ceramics are normally fabricated from expensive high quality AlN, $Si_3N_4$, $SiO_2$, and $Al_2O_3$ powders, and hence their applications are limited due to the high cost. Consequently, the alumina ceramic is still the most extensively used wear resistant lining materials. We have developed a new metal–Sialon system of Fe/Mo–Sialon by hot pressing [12–14]. The discrete FeMo alloy phase can highly toughen the Sialon based ceramic. This ceramic matrix composite has good mechanical properties but is still high-cost. So this paper aims to develop a Fe–Sialon ceramic composite by nitridation-reaction sintering from low cost ferro-silicon alloy and industrial alumina powders, and characterize the phase composition, mechanical properties, microstructure and high temperature erosion resistance of the as-fabricated composite.

## 2. Experimental procedure

### 2.1. Raw materials

The main starting materials were as follows: FeSi75 ferro-silicon alloy powders (chemical composition wt.%, Fe 21.041, Si 76.400, Al 1.230, P 0.012, Ca 1.240, C 0.070, S 0.007, grain size <74 μm), commercially α-$Al_2O_3$ powders (99.6 wt.% pure, grain size 2–3 μm,

* Corresponding author. Tel.: +86 10 8232 2186; fax: +86 10 8232 2186.
*E-mail address:* huang118@cugb.edu.cn (Z.-H. Huang).

Peer review under responsibility of The Ceramic Society of Japan and the Korean Ceramic Society.

Production and hosting by Elsevier

2187-0764 © 2013 The Ceramic Society of Japan and the Korean Ceramic Society. Production and hosting by Elsevier B.V. All rights reserved.
http://dx.doi.org/10.1016/j.jascer.2013.05.001

**Table 1**
Batch formula of the starting powders.

| Sample code | F1 | F2 | F3 | F4 | F5 | F6 |
|---|---|---|---|---|---|---|
| FeSi75 alloy content, wt.% | 100 | 80 | 60 | 40 | 20 | 0 |
| $\alpha$-$Al_2O_3$ content, wt.% | 0 | 20 | 40 | 60 | 80 | 100 |

Aluminum Corporation of China, Ltd.), and industrial $N_2$ (99.99 wt.% pure). The particle sizes of the raw material powders are provided by the manufacturers and confirmed by the Laser Particle Size Analyzer (Bettersize, China).

### 2.2. Processing details

The sample codes and batch formula are listed in Table 1. The nominal $Z$ values of β-Sialon in samples F2, F3, F4 and F5 are 0.9, 1.9, 2.8 and 4 (with excessive alumina addition). The raw material powders were mixed by high-speed ball milling (planetary ball mill) in an $\phi$ 80 mm × 100 mm high purity alumina ceramic jar for 2 h. Agate balls of 3–8 mm in diameter were employed as the grinding medium and water as the milling solvent. Then the mixtures were dried using a rotary evaporator, and then pressed to cylinder pellets of 20 mm in diameter and 20 mm in height under 100 MPa pressure. Then the green bodies were further densified by cold isostatic pressing under a pressure of 200 MPa for 60 s, dried at 70 °C for 10 h, and finally reaction-sintered in a 0.9 MPa flow nitrogen-gas in a multifunctional atmosphere sintering furnace (Model No. FVPHP-R-5, Fuji Dempa Kogyo Co., Ltd., Japan). The sintering schedule was 1200 °C × 0.5 h, 1350 °C × 0.5 h, 1480 °C × 0.5 h and 1700 °C × 3 h. The heating rate was 40 °C/min from the room temperature to 1200 °C and 10 °C/min from 1200 °C to 1700 °C.

### 2.3. Characterization

The apparent porosities of the reaction-sintered samples were measured by the Archimedes' method. The bending strengths were determined by the three-point bending test with a 20 mm span at a crosshead speed of 0.5 mm/min at room temperature. In order to improve the reliability of the test results, all those samples were polished with a final surface finish of 1 μm and 6 tests were conducted for each type of sample. The Rockwell hardness (HRA) was also measured under a load of 60 kg and holding time of 10 s. The crystalline phases were examined by X-ray diffractometer (XRD) (Bruker, D8 Advance, Germany) with Cu Ka1 radiation (λ = 1.5406 Å) as X-ray source. To estimate the actual $Z$ values of the β-Sialon in the as-fabricated Fe–Sialon composites, the crystal lattice constants were calculated by the following equation [15]:

$$d_{hkl} = \frac{a}{\sqrt{(4/3)(h^2 + hk + k^2) + (a/c)^2 \cdot l^2}}$$

where $a$ and $c$ are the lattice parameters of the β-Sialon, $d_{hkl}$ is the space distance between the reflection planes ($hkl$). Parameters $a$ and $c$ were calculated using the (2 0 0), (1 0 1) and (2 1 0) reflections. The $Z$ values of β-Sialon phases in the composites were obtained from the mean values of $Z_a$ and $Z_c$ calculated from the following equation [15]:

$$a = 7.603 + 0.0296Z \text{ Å}$$

$$c = 2.907 + 0.0255Z \text{ Å}$$

As erosion-wear targets, the as-fabricated Fe–Sialon and the control material of alumina ceramic were machined to 15 mm thick followed by polishing with a diamond abrasive disk and ultrasonic cleaning in anhydrous ethanol. Then erosion tests were performed

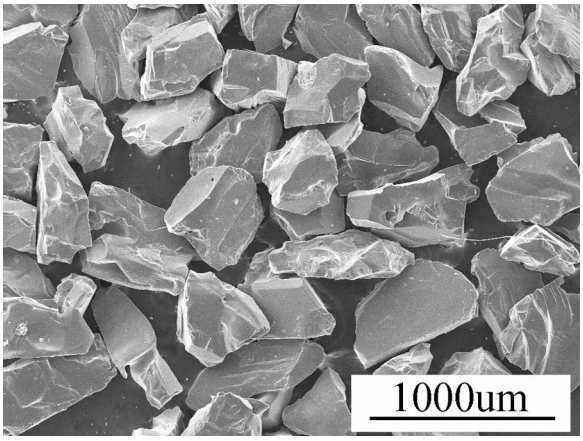


**Fig. 1.** Morphology of SiC sand-blasting particles.

by an in-house designed high-temperature (up to 1400 °C) solid particle erosion equipment in accordance with ASTM G76-04, whose schematic diagram is shown in our previous study [16]. The nozzle and target are within the chamber of the furnace. The recrystallized silicon carbide erosion chamber is for protecting the heating unit and furnace lining from erosion damage. Black silicon carbide grits (97% of particles are within the size range of 325–830 μm) were used as impact particles. The grits have angular morphologies as shown in Fig. 1. The media gas was compressed air with a pressure of 0.46 MPa. The particle flux was 60 g $min^{-1}$. The impingement angle of gas-particle stream on the target was 90°. The impact velocity was 50 m/s measured by the rotating double-discs method [17]. The impact particles are accelerated in an air stream down a glass tube (diameter 10 mm) and corundum ceramic nozzle (diameter 20 mm) to impact the targets at 25 °C, 1000 °C, 1200 °C and 1400 °C. The stand-off distance, from the end of the nozzle to the surface of the target, was 10 cm. The duration of each test was 5 min to allow 300 g of SiC particles impacting the target surface. The erosion resistance was characterized with the volume erosion rate, which was defined as the volume loss of specimen material divided by the total mass of abrasive particles that impacted the specimen ($mm^3$ $g^{-1}$) as shown below [18].

$$\text{volume erosion rate} = \frac{\text{average mass loss}}{\text{test time}} \times \frac{1}{\text{particle flux}} \times \frac{1}{\text{specimen density}}$$

In order to analyze the microstructure, alloy phase distribution and material removal mechanism, the fracture and eroded surfaces were observed by scanning electron microscope (SEM, JSM-6460, Japan) with an energy dispersive spectroscopy detector (EDS, INCAX-Sigh, Oxford, UK).

## 3. Results and discussion

The XRD pattern in Fig. 2 presents that the main crystalline phases in ferro-silicon alloy are Si and $FeSi_2$. As shown in Fig. 3, Fe–Sialon ceramic composite contains β-Sialon ($Si_{6-Z}Al_ZO_ZN_{8-Z}$) and $Fe_3Si$ phases. The positions of diffraction peaks of β-Sialon phase were shifted to the high-angle direction with increasing alumina addition, which was attributed to the changed interplanar space $d$. It is well known that the $Z$ value of β-Sialon reflects the substitution extent of Si, N atoms by Al, O atoms, and the average value of Al—N bond (1.87 Å) and Al—O bond (1.75 Å) is longer than the Si—N bond (1.74 Å), which is related to the lattice parameters

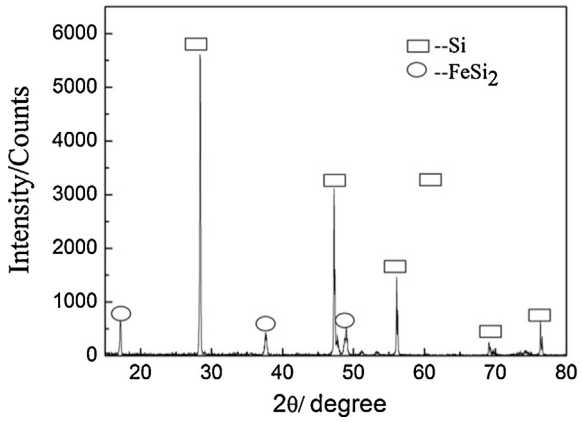


**Fig. 2.** XRD pattern of FeSi75 alloy powders.

and interplanar space [19]. Thus, the $Z$ value of β-Sialon is in proportion to the interplanar space $d$. β-Sialon phases formed in the samples F2, F3 and F4 have the actual $Z$ values of 1.0, 2.1 and 2.9, respectively, which are slightly higher than the nominal ones of 0.9, 1.9 and 2.8. That is to say, the real substitution extent of Al, O atoms to Si, N atoms is higher than expected. This phenomenon could be explained by the following analysis. The element Si in $FeSi_2$ was not totally consumed to form Sialon, as some amount of Si existed in the new phase of $Fe_3Si$ after nitridation-sintering. So the reactant Al/Si ratio is bigger than the nominal one, which resulted in the mild increase of real $Z$ values compared with the nominal ones. For sample F5 with excessive addition of alumina, the nominal $Z$ value of β-Sialon is 4, but the real one is only 3.2. Thus, for the present ferro-silicon alloy and alumina reactant system, the alumina substitution extent is limited and $Si_2Al_4O_4N_4$ ($Z = 4$) cannot be generated.

Thermodynamic analysis was carried out to understand the formation mechanism of β-Sialon from the nitridation-reaction sintering of ferro-silicon alloy and alumina. The Gibbs energies of $\Delta r_{(1)}G^{\theta}$ and $\Delta r_{(2)}G^{\theta}$ are both minus and chemical equations (1) and (2) can take place when the reaction temperature is below 2223 K (1950 °C). So the Si and $FeSi_2$ in ferro-silicon alloy could be nitridized to produce $Si_3N_4$, which has been proved in our previous study [20]. Then $Si_3N_4$ reacts with $Al_2O_3$ and $N_2$ to form β-Sialon

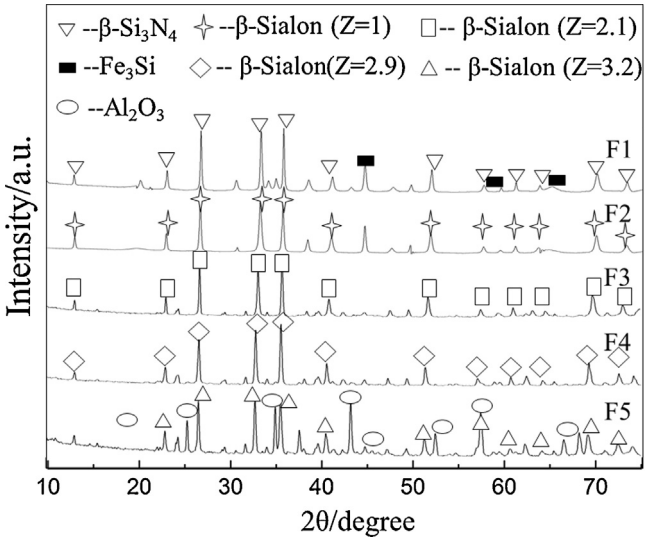


**Fig. 3.** XRD patterns of Fe–Sialon ceramic composites.

when the temperature goes up over 1443 K (1170 °C) and $\Delta r_{(3)}G^{\theta}$ becomes minus, taking $Z = 3$ for example [21]. It has been reported that β-Sialon can be produced from $Si/Si_3N_4$, $Al_2O_3$ and $N_2$ [22–24]. In addition, Si, $Al_2O_3$, $N_2$ and $O_2$ (impurity) could directly form an intermediate phase of O-Sialon that can transform to β-Sialon [25]. This may be another possible pathway for β-Sialon formation in this study. It should be noted that Fe is beneficial to promote the nitridation of Si and the formation of Sialon [26]. So ferro-silicon alloy powders would be the promising raw materials for fabricating industrial Sialon based ceramic composites.

$$3Si + 2N_2 = Si_3N_4 \quad (1)$$

$$\Delta r_{(1)}G^{\theta} = -744.752 + 0.335T \ \ (\text{kJ mol}^{-1})$$

$$(9/5)FeSi_2 + 2N_2 = Si_3N_4 + (3/5)Fe_3Si \quad (2)$$

$$\Delta r_{(2)}G^{\theta} = -693.552 + 0.226T \ \ (\text{kJ mol}^{-1})$$

$$2Si_3N_4 + 3Al_2O_3 + N_2 = 2Si_3Al_3O_3N_5 + (3/2)O_2 \quad (3)$$

$$\Delta r_{(3)}G^{\theta} = 960.86 - 0.666T \ \ (\text{kJ mol}^{-1})$$

The apparent porosity, bending strength and Rockwell hardness of Fe–Sialon ceramic composites and alumina ceramic were determined and the results are displayed in Fig. 4 [21]. As shown in Fig. 4(a), the apparent porosity of Fe–Sialon ceramic samples ranges from 6% to 12% that is much higher than that (0.5%) of alumina ceramic. Fig. 4(b) and (c) presents that the bending strength and Rockwell hardness are close to those (184 MPa and 85 HRA) of alumina ceramic and slightly increase with raising the alumina content. For the Fe–Sialon composites, sample F2 exhibits the highest bending strength due to its lowest porosity.

Fig. 5 shows the microstructure features of reaction-sintered Fe–Sialon ceramic composite mainly containing β-Sialon and $Fe_3Si$ (one kind of ferro-silicon alloys) phases. As can be seen in Fig. 5(a) and (c), angular $Fe_3Si$ alloy particles (white phase) with a diameter of about 30 μm distribute discretely in the ceramic matrix and are located at the grain boundaries of elongated Sialon crystals. The Sialon grains interlock with each other and vary in size. Note that spherical $Fe_3Si$ alloy particles of 1–3 μm in diameter can be found in the eroded surface of Fe–Sialon samples, as shown in Fig. 5(d). It suggests that they were erosion worn by the impact particles evidenced by their shape change from angular to spherical. $Fe_3Si$ alloy is brittle at room temperature, but it will become more ductile at high temperatures below its melting point of 1300 °C [27]. In other words, the $Fe_3Si$ alloy phase could deform to some extent when eroded by the SiC grits at high temperature, which may consume the impacting energy and reduce the erosion damage to the Fe–Sialon composite. Although the micro-cut of the erodent grits would make $Fe_3Si$ alloy particles smaller, their deformation may still occur at the same time. The photos of erosion-worn samples are presented in Fig. 6. Round erosion pits can be found in the surfaces. The depths of the erosion pits look different, which indicates that there should be various erosion rates for the samples.

Fig. 7 shows the volume erosion rate of Fe–Sialon and $Al_2O_3$ ceramics as a function of the testing temperature. Except sample F1, the volume erosion rates of Fe–Sialon ceramics mainly tend to increase initially, reach the peak value at 800 °C, and then decrease with increasing temperature. Sample F4 shows much higher erosion rate than all the other samples at the temperature ranging from 25 °C to 1200 °C. The reason may be related to the defects (aggregates, macro pores, etc.) resulting from the non-uniform mixed starting powders. For sample F3 with 60 wt.% ferro-silicon alloy addition, the erosion rate value increases from

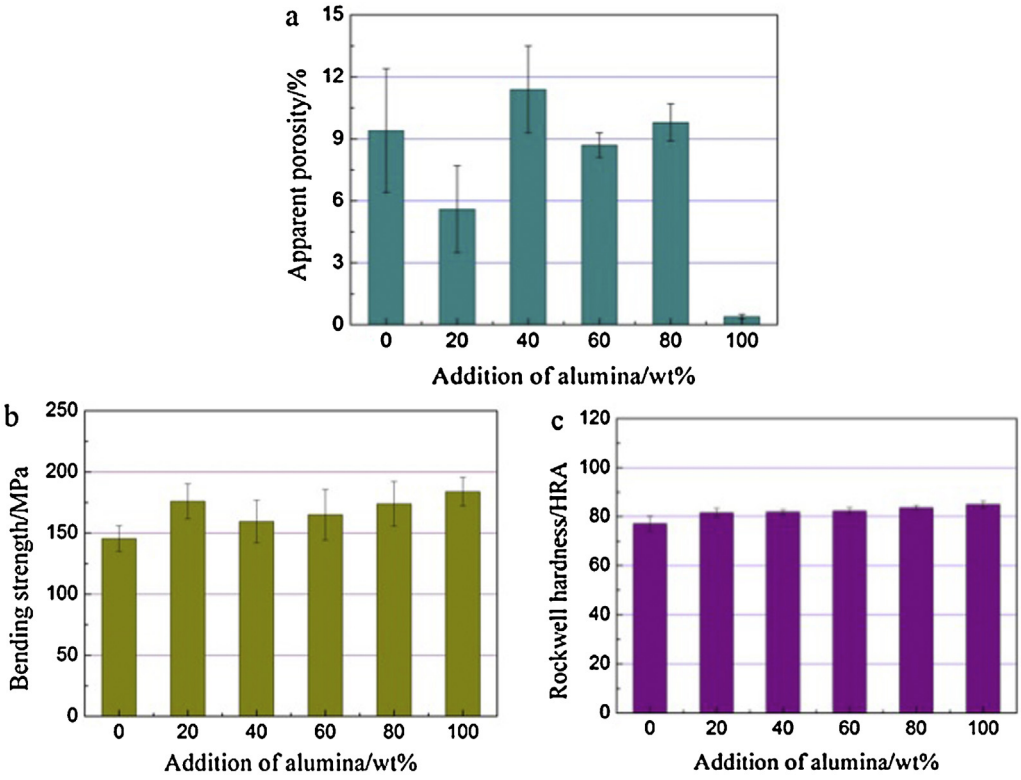


**Fig. 4.** The effects of alumina mass addition on (a) apparent porosity; (b) bending strength; and (c) Rockwell hardness of Fe–Sialon ceramic composites.

$0.46 \pm 0.07\ mm^3/g$ at room temperature to $1.38 \pm 0.10\ mm^3/g$ at 800 °C, then sharply decreases to $0.64 \pm 0.13\ mm^3/g$ at 1200 °C. It indicates that the maximum erosion took place at 800 °C. The reason may be related to the declined hardness of Fe–Sialon ceramics. The temperature dependence of the erosion rate for some ceramics has been reported in the literature. Alman et al [28] performed the erosion tests on $Si_3N_4$ and $Si_3N_4$–$SiO_2$ ceramics at 25 °C, 180 °C, 500 °C, 700 °C and 900 °C, and the results show that the erosion rate for the $Si_3N_4$–$MoSi_2$ composite initially increase slightly with increasing test temperature up to 700 °C (ie from 4.1 to 4.9 $mm^3/g$), then decreased to 2.9 $mm^3/g$ at 900 °C. For $Si_3N_4$ ceramic, the erosion rate reaches the highest value at 500 °C, and then decreases to the lowest value at 700 °C. Such a variation tendency of the erosion rate is similar to the findings in this study. Ham et al [29] reported

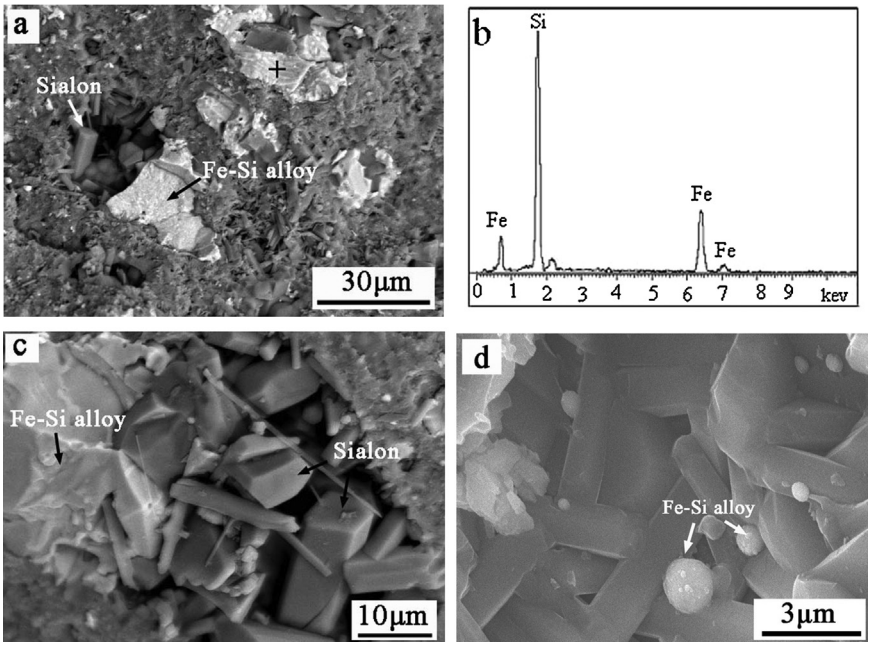


**Fig. 5.** SEM images showing the microstructure of Fe–Sialon ceramic: (a) fracture surface; (b) the EDS pattern of the area marked by '+' in (a); (c) fracture surface morphology with high magnification; and (d) eroded surface morphology.

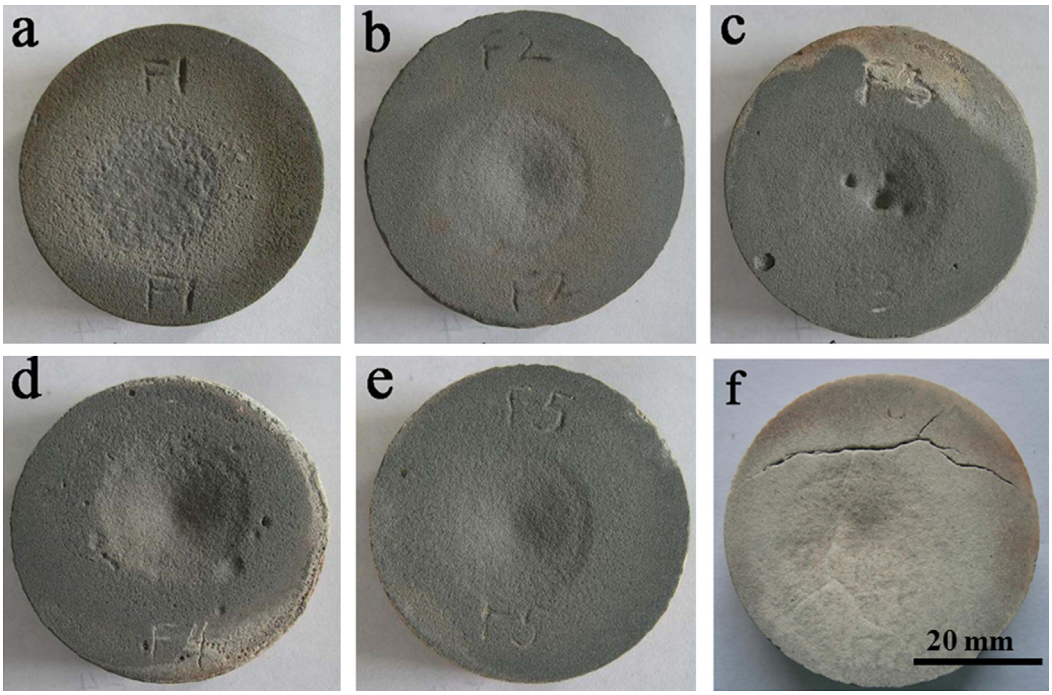


**Fig. 6.** Photos of Fe–Sialon composites (a) F1; (b) F2; (c) F3; (d) F4; (e) F5; and (f) $Al_2O_3$ ceramic samples impacted by SiC particles at 1000 °C.

that the erosion rate of the SiC continuous fibers reinforced calcium aluminosilicate glass–ceramic composite also presents a tendency of increasing first (up to the highest value at 400 °C) and decreasing later versus the test temperature from 20 to 726 °C. The volume erosion rates of Fe–Sialon samples (F1–F3) are all lower than that of $Al_2O_3$ ceramic at 1200 °C. In other words, Fe–Sialon ceramics show better erosion resistance at the high temperature of 1200 °C. The mechanical properties are close to those of commercial $Al_2O_3$ ceramic as displayed in Fig. 4. Fe–Sialon ceramic based composite with good erosion resistance and low cost, could be an alternative candidate of wear resistant materials used at high temperatures.

In order to understand the material removal mechanisms, the centers of eroded pits were observed by SEM. Fig. 8 shows typical eroded surface morphologies of Fe–Sialon ceramics at 1000 °C. As can be seen in Figs. 8(a)–(c), there are some cracks in the intergranular phase after impacted by SiC particles. The material was removed by fragmenting and chipping due to the continuously impacting of SiC particles. It is obvious that brittle fracture is the primary erosion mechanism.

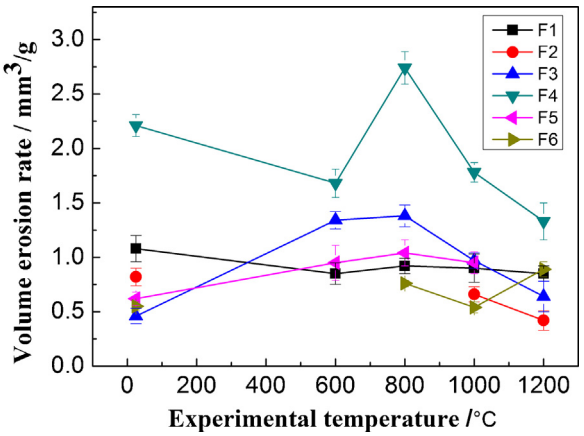


**Fig. 7.** The volume erosion rates of Fe–Sialon and $Al_2O_3$ ceramic samples versus the test temperatures (25 °C, 600 °C, 800 °C, 1000 °C, and 1200 °C).

At elevated temperatures, it is also possible for Fe–Sialon ceramics to exhibit plastic erosion features of plastic deformation and ploughing groove as denoted by arrows and circles in Figs. 8(c) and (d). Due to the impurities in the ferro-silicon alloy powder, it is reasonable that glassy phase exists in the as-fabricated Fe–Sialon ceramics. The intergranular glassy phase will soften and show plastic property to some extent with increasing temperature. And the $Fe_3Si$ alloy phase distributing discretely in the Sialon ceramic matrix becomes ductile at high temperature. That may be the reason why ductile erosion features appear. And the effect of intergranular glass on the erosion resistance of slag α-Sialon ceramic has been investigated [10]. It is believed that an optimum amount of intergranular glass may improve the erosion resistance of α-Sialon ceramics. In this study, the ductile erosion damage is also responsible for the material removal.

Fig. 9 shows the erosion morphologies of Sialon crystals in Fe–Sialon ceramics and $Al_2O_3$ crystals in sample F6 (control material of alumina ceramic) at 1000 °C. It is noted that the elongated Sialon crystals are exposed after the intergranular glass removed by continuous impacting of SiC erodent particles. The weak intergranular phase in the edges of the micro pores formed during reaction-sintering are easily fragmented and removed from the samples. The exposed strong elongated Sialon crystals can endure the impact of SiC particles and the overall material loss through erosion is sequentially reduced. It indicates to some extent that interlacing elongated Sialon crystals bond well with each other. However it is believed that some Sialon crystals were dislodged during the erosion test at room temperature [10].

It can also be seen that Sialon crystals are crack free without crushing or fracturing after impacted by SiC particles as shown in Fig. 9. On the contrary, as can be seen from Fig. 9(f), $Al_2O_3$ crystals crack and fracture after the erosion test under the same conditions. It has been demonstrated that Sialon crystals show better the erosion resistance than $Al_2O_3$. It can be concluded that the

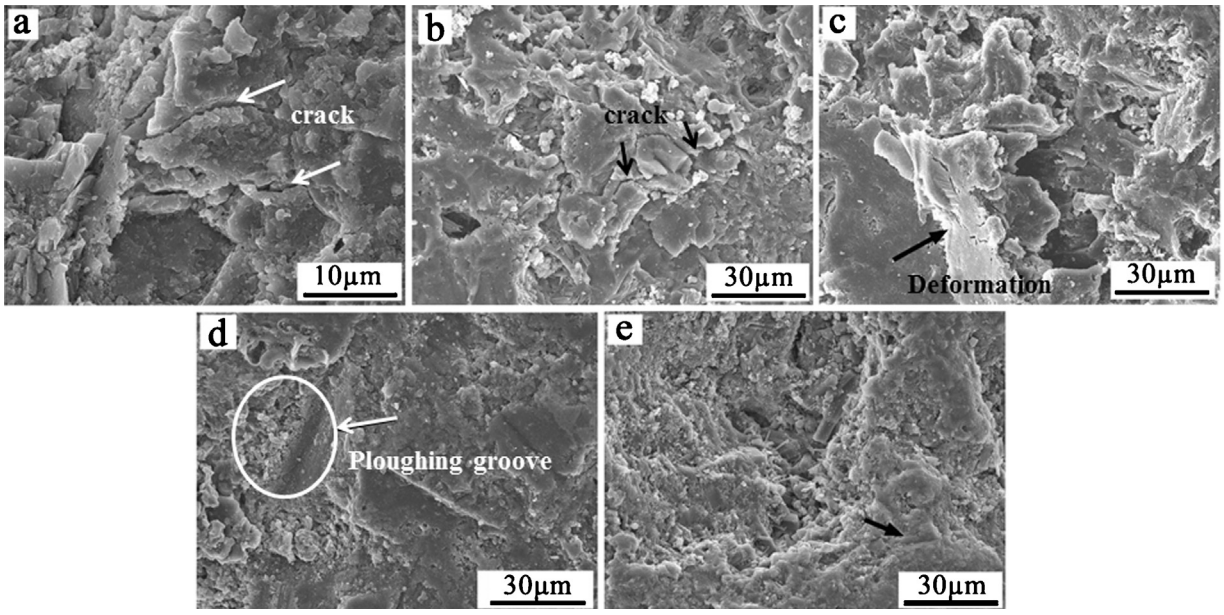


**Fig. 8.** Typical eroded surface morphologies of Fe–Sialon ceramic samples impacted by SiC particles: (a) 25 °C; (b) 600 °C; (c) 800 °C; (d) 1000 °C; and (e) 1200 °C.

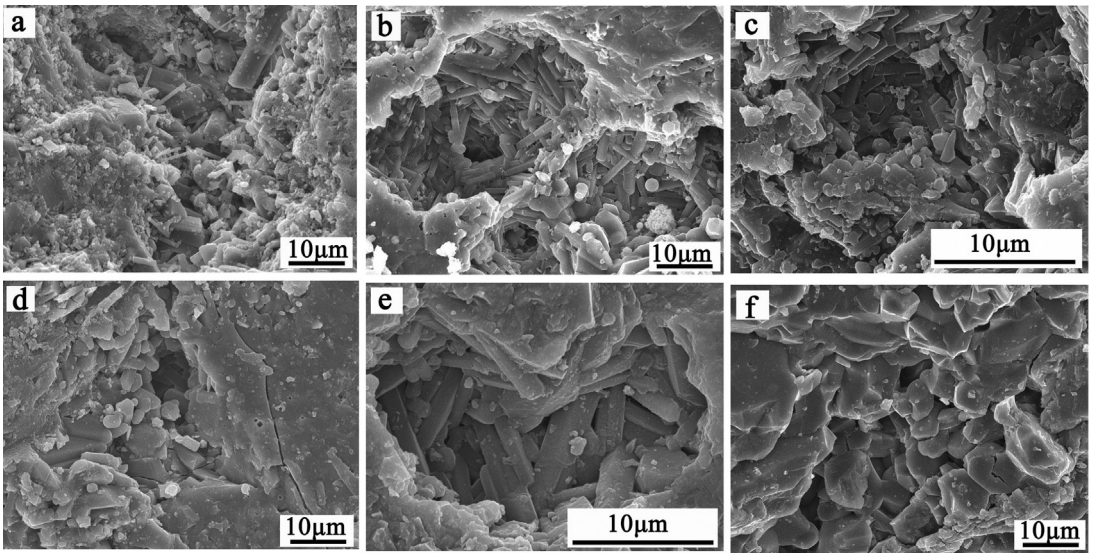


**Fig. 9.** Typical erosion surface images of Sialon crystals in Fe–Sialon ceramics and $Al_2O_3$ crystals in sample F6 impacted by SiC particles at 1000 °C: (a) F1; (b) F2; (c) F3; (d) F4; (e) F5; and (f) F6.

primary material removal mechanisms are fracture and chipping of intergranular glass phase, as well as Sialon crystals dislodging.

## 4. Conclusions

A novel ceramic matrix composite of Fe–Sialon has been successfully fabricated by nitridation-reaction sintering from ferrosilicon alloy and alumina powders. The composite mainly contains β-Sialon and $Fe_3Si$ phases. $Fe_3Si$ alloy particles distribute discretely in ceramic matrix and are located at the grain boundaries of interlocked elongated Sialon crystals. The bending strength and Rockwell hardness gradually increased with increasing the alumina addition. The erosion rate of Fe–Sialon ceramic is highly dependent on the testing temperature. The minor erosion took place at room temperature or 1200 °C, while the major erosion occurred at 600–1000 °C. Fe–Sialon ceramic composite shows better erosion wear resistance than $Al_2O_3$ ceramic at 1200 °C due to the interlocked elongated strong Sialon grains and discrete intergranular $Fe_3Si$ alloy phase.

## Acknowledgements

The authors highly appreciate National Natural Science Foundation of China (Grant Nos. 50572098, 50802091, and 50972134), Fundamental Research Funds for the Central Universities (Grant Nos. 2009PY09, 2009PY10 and 2010ZD12) and University of Western Australia, ECM Faculty Small Research Development Grant 2012–2013. J.-Z. Yang is supported by Innovation and Technology Fund for Postgraduate of China University of Geosciences (Beijing). Z.-H. Huang is supported by Gledden Visiting Senior Fellowship from University of Western Australia in 2010.

## References


[1] M.I. Jones, K. Hirao, H. Hyuga, Y. Yamauchi and S. Kanzaki, J. Eur. Ceram. Soc., 23, 1743–1750 (2003).
[2] M.I. Jones, K. Hirao, H. Hyuga, Y. Yamauchi, Z.-J. Shen and M. Nygren, Wear, 257, 292–296 (2004).
[3] S. Kurama, I. Schulz and M. Herrmann, J. Eur. Ceram. Soc., 29, 155–162 (2009).
[4] M.I. Jones, H. Hyuga, K. Hirao and Y. Yamauchi, J. Eur. Ceram. Soc., 24, 3271–3277 (2004).
[5] Z.-H. Xie, M. Hoffman, R.J. Moon, P.R. Munroe and Y.-B. Cheng, Wear, 260, 387–400 (2006).
[6] V.X. Lima Filho, J.P. Davim, C.A. Cairo and J.M.F. Ferreira, Int. J. Refract. Met. Hard Mater., 27, 647–652 (2009).
[7] B. Basu, J. Vleugels, M. Kalin and O. Van Der Biest, Mater. Sci. Eng. A, 359, 228–236 (2003).
[8] W.G. Zhang, W.-M. Liu and L.-G. Yu, Tribol. Int., 33, 769–775 (2000).
[9] W.-W. Chen, J. Steel, Y. Zhang, J.-X. Jiang, Y.-B. Cheng, P.-L. Wang and D.-S. Yan, J. Eur. Ceram. Soc., 24, 2847–2851 (2004).
[10] Y. Zhang, Y.-B. Cheng and S. Lathabai, J. Eur. Ceram. Soc., 21, 2435–2445 (2001).
[11] D.-M. Liu, J.-T. Lin and R.R. Lee, Ceram. Int., 24, 217–221 (1998).
[12] J.-Z. Yang, Z.-H. Huang, M.-H. Fang, Y.-G. Liu, J.-T. Huang and J.-H. Hu, Scripta Mater., 61, 632–635 (2009).
[13] J.-Z. Yang, Z.-H. Huang, X.-Z. Hu, M.-H. Fang, Y.-G. Liu and J.T. Huang, Mater. Sci. Eng. A, 528, 2196–2199 (2011).
[14] Z.-H. Huang, J.-Z. Yang, Y.-G. Liu, M.-H. Fang, J.-T. Huang, H.-R. Sun and S.-F. Huang, J. Am. Ceram. Soc., 95, 859–861 (2012).
[15] T. Ekstrom and M. Nygren, J. Am. Ceram. Soc., 75, 259–276 (1992).
[16] J.-Z. Yang, M.-H. Fang, Z.-H. Huang, Y.-G. Liu, H.-R. Sun, J.-T. Huang and X.-C. Li, J. Eur. Ceram. Soc., 32, 283–289 (2012).
[17] A.W. Ruff and L.K. Ives, Wear, 35, 195–199 (1975).
[18] ASTM G76-04. Standard test method for conducting erosion tests by solid particle impingement using gas jets.
[19] K. Kishi, S. Umebayashi, E. Tani, K. Shobu, R. Pompe and A. Kristffersson, J. Eur. Ceram. Soc., 18, 2015–2018 (1998).
[20] J.Z. Yang, Z.H. Huang, M.H. Fang, Y.G. Liu and X.X. Wu, Key Eng. Mater., 368–372, 1123–1125 (2008).
[21] J.B. Tu, Research on Silicon (aluminium)-corundum-silicon nitride composites, University of Science and Technology of Beijing, Beijing (2004) (PhD thesis) (in Chinese).
[22] T. Włodek, M. Sopicka-Lizer, H. Gocmez and C. Duran, J. Eur. Ceram. Soc., 27, 739–742 (2007).
[23] H.X. Zhu, C.J. Deng, J.Y. Li, C. Chen and Y.P. Zhang, Chin. Mater. Sci. Tech. Equip., 5, 49–52 (2007) (in Chinese).
[24] A.D. Mazzoni and E.F. Aglietti, Mater. Chem. Phys., 48, 41–47 (1997).
[25] H.J. Wen, Research on the Basic application of alusite, University of Science, Technology of Beijing, Beijing (1997) (PhD thesis) (in Chinese).
[26] S.F. Huang, Z.H. Huang, M.H. Fang, Y.G. Liu, J.T. Huang and J.Z. Yang, Cryst. Growth Des., 10, 2439–2442 (2010).
[27] Y. Pan and J.L. Baptista, J. Am. Ceram. Soc., 83, 2919–2924 (2000).
[28] D.E. Alman, J.H. Tylczak, J.A. Hawk and M.G. Hebsur, Mater. Sci. Eng. A, 261, 245–251 (1999).
[29] A.L. Ham, J.A. Yeomans and J.F. Watts, Wear, 233, 237–245 (1999).